Turbulent three-phase simulations of the circumgalactic medium

Zewei Wu[1,2]⋆, Hitesh Kishore Das[1,3]†, Max Gronke[1]‡

[1]*Max Planck Institute for Astrophysics, 85748 Garching b. München, Bavaria, Germany*
[2]*Department of Astronomy & Astrophysics, The University of Chicago, Chicago 60637, IL, USA*
[3]*Ludwig-Maximilians-Universität München, 80539 München, Bavaria, Germany*

ABSTRACT

In this work, we investigate the survival and destruction criteria of CGM clumps. We focus on the three-phase hydrodynamical simulations of concentrated cold gas in a hot medium.

This project is useful for constraining the mass, energy, and momentum transfers of different gas phases, as well as for quantifying the phase interaction terms (energy exchange, drag, etc.), which are useful quantities for larger, multifluid simulations such as `AREPO`.

Key words: galaxies: CGM, galaxies: ISM, galaxies: intergalactic medium

1 INTRODUCTION

JW: THIS SECTION IS NOT REVISED FROM THE WRITE-UP

In astrophysics, many systems are "multiphase", where cold, dense matter coexists within a predominantly hot environment. Examples include:

• **Intracluster Medium (ICM)**: This vast gas within the Universe's largest structures, up to $\sim 10^{15}$ solar masses, is primarily hot, around $\sim 10^7 - 10^8$ K. However, observations reveal Hα filaments suggesting $\sim 10^4$ K gas and even colder molecular gas.

• **Circumgalactic Medium (CGM)**: Surrounding galaxies, the CGM contains gas at $\sim 10^6$ K, with cold clumps below $\lesssim 10^4$ K. This cold gas fuels star formation, shaping CGM-regulated galaxies.

Other examples include the interstellar medium, the surrounding massive black holes, or other accretion disks. Or outside the extragalactic context also the coronal rain – observed in our own Sun – which is again $\sim 10^4$ K material falling in a hot $\sim 10^6$ K corona. These systems are crucial in understanding diverse astrophysical processes. These examples how important of a role multiphase gas plays in astrophysics. Thus, understanding its dynamics from basic principles is crucial in order to understand larger systems such as galaxies. (Tumlinson et al. 2017)

One of the most commonly used ways to understand multiphase gas is with hydrodynamical simulations such as `AREPO`. However, these simulations tend to be large and complicated, involving multifluid simulations and with magnitudes spanning across 20 orders. Further, despite the simplicity of the initial conditions, the system develops highly non-linear multiphase turbulence very soon. As a result, a lot of the microphysics with respect to the mass, energy, and momentum transfers is still ill-understood.

⋆ E-mail: wuz25@uchicago.edu
† E-mail: hitesh@mpa-garching.mpg.de
‡ E-mail: maxbg@mpa-garching.mpg.de

Further more, observations () and cosmological simulations () alike have uncovered cold, molecular gas in the CGM, at temperatures ~ 800 K. Though there has yet to be convergence amongst simulations in the exact amount of cold gas (Faucher-Giguère et al. 2010; van de Voort et al. 2019; Hummels et al. 2019; Nelson et al. 2020; Bennett & Sijacki 2020).

In this project, we focus on zoom-in boxes in `Athena`++, using a set of three-phase simulations of concentrated cold gas in a hot medium. This scenario is crucial to understand as it directly pertains to the survival or destruction of the cold gas phase, which is abundantly observed in the CGM. Our specific goals are:

(i) To build upon previous results in Das & Gronke (2024), which focused on 2-phase gas, and introducing a wider temperature range from $T_{\rm floor} = 800 \sim T_{\rm ceil} = 4 \times 10^6$ K.

(ii) To test the analytical destruction / survival criteria for different cloud and hot gas temperatures.

(iii) To investigate the numerical convergence of different temperature ranges to draw conclusions on physical effects.

2 METHODOLOGY

For our hydrodynamical simulation, we use the `Athena`++ code (Stone et al. 2020). We use the default HLLC Reimann solver, applying Piecewise Linear Method (PLM) on primitive variables. We use a second-order Runge-Kutta time integrator, adiabatic EOS, and a cartesian geometry with periodic boundary conditions.

2.1 Turbulence

We use a simulation setup similar to the hydrodynamical (HD) runs of Das & Gronke (2024). We initialize the box of size $L_{\rm box}$, with isobaric gas at uniform density ($\rho_{\rm hot}$) and temperature ($T_{\rm hot} = 4 \times 10^6$ K), with solar metallicity and hydrogen composition. We drive the turbulence

impulsively using Ornstein-Uhlenbeck (OU) process (Schmidt et al. 2004; Eswaran & Pope 1988).

We run the simulation for 10 eddy-turnover timescales (t_{eddy}) without radiative cooling, for the turbulence to cascade down the Kolmogorov scales and reach equilibrium kinetic energy. By the end of the turbulent driving phase, the energy influx is dissipated into thermal energy due to the adiabatic equation-of-state. Therefore, we then scale the average ambient temperature of the box to the desired T_{hot} before introducing the cloud.

2.2 Cold cloud

We introduce a spherical cold cloud after driving turbulence until a steady-state is achieved with the desired Mach number. We maintain $L_{box}/R_{cl} = 20$ with resolution of 128^3 cells for runs with $T_{floor} = 8000$ K; and $L_{box}/R_{cl} = 50$ with resolution of 256^3 cells for runs with $T_{floor} = 800$ K. The higher L_{box}/R_{cl} is to maintain a reasonably high hot gas mass fraction in the box.

We enforce temperature floors at $T_{floor} = 8000$ and 800 K, to allow for the survival of two-phase and three-phase gases, respectively, according to the cooling curve, which we discuss more in Section 2.3.

After adding the cloud, the simulations are restarted and run until $\sim 10\times$ the cloud crushing time t_{cc} or the eddy time t_{eddy}, whichever is larger. Here, t_{cc} represents the time it takes for a shock to propagate through and compress the cold cloud, and t_{eddy} is the characteristic timescale associated with turbulent motion in the box.

The survival and destruction of the cold cloud in a hot, turbulent medium is subject to the strength of mixing and cooling. Whereas mixing tends to destroy the gas, cooling tends to preserve and grow the gas phase from an initial seed.

Besides mixing, the destruction of cold gas can also be influenced by the increased cooling time, as well as the depletion of gas phases due to the limited box size, or reaching the pressure floor of the simulation. The first factor is a genuine physical consideration depending on box size, while the latter two are confounding factors that are contingent on our simulation setup. As such, we halt the simulation when the following conditions are achieved: either more than 0.5% of all cells in the box have pressure $< 2 \times P_{floor}$, if the hot gas mass depletes to $< 20\%$, or the cold to $< 5\%$. Thus, the growth and destruction patterns of the cold & warm gas in the box should only be reflective of the strength of cooling and mixing timescales. We expand further upon this conclusion in Section 5.2.

2.3 Radiative Cooling

We assume a collisional ionizational equilibrium for cooling rates. Similar to previous similar works (Gronke et al. 2022; Das & Gronke 2024), we use the method from Townsend (2009) for computing the radiative losses. We assume solar metallicity and use a piecewise-powerlaw cooling function from. We adopt a cooling curve for solar metallicity similar to Gronke et al. (2022), fitted with 70 segments of piecewise powerlaws, down to $T_{floor} = 100$ K.

We choose 800 K as temperature floor for the three phase gas, because it probes the regime of flattened molecular cooling which is of interest, while maintaining a low enough overdensity of the cold gas to be numerically achievable.

We normalize our cloud radii by the shattering length $l_{shatter} = \min(c_s t_{cool})$, which corresponds to $T \sim 2 \times 10^4$ K, which roughly matches the temperature corresponding to the minimum cooling time in our simulation.

Fig. 1 shows the cooling function ($\Lambda(T)$) on the left y-axis as
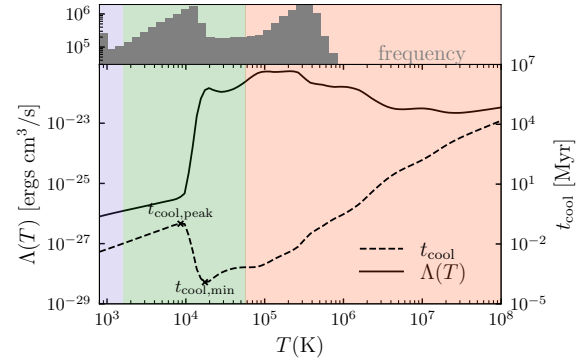
Figure 1. The cooling function $\Lambda(T)$ (*solid line, left axis*), and the cooling time t_{cool} (*dashed, right axis*) of a particular cloud crushing setup with floor temperature $T_{floor} = 800$ K and hot gas density $\rho_{hot} = 0.1$ mp/cm^3. The local peak $t_{cool,peak}$ and minimum $t_{cool,min}$ of the cooling time are labeled. The three shaded regions mark the temperature range for the cold $T_{cloud} < T < 2\times T_{cloud}$ (*blue*), warm $2 \times T_{cloud} < T < T_{mix}$ (*green*), and hot gas temperatures $T_{mix} < T < T_{ceil}$ (*red*) used in this study. These correspond to the temperature distribution of a simulation snapshot shown on top of the figure, where the three stable phases are clearly separated.

the solid line and an example of cooling timescale (t_{cool}) on the right y-axis as the dashed line, between 800K and 10^8K. We assume isobaricity and a hot gas density of $\rho_{hot} = 0.1$ mp/cm^3 at $T_{hot} = 4 \times 10^6$ K. The temperature range is split into three regimes, corresponding to the three phases of gas. We define cold gas phase as gas with temperature in $[T_{cloud}, 2 \times T_{cloud}]$, shown in blue, warm gas phase with temperature in $[2 \times T_{cloud}, T_{mix}]$, shown in green, and hot gas phase with temperature above T_{mix}, shown in red. Here, T_{mix} refers to the geometric mean of the cold and hot gas temperature, i.e. $\sqrt{T_{cold}T_{hot}}$ **HD: Cite Begelmann**. The top panel of Fig. 1 shows the number distribution of the temperature distribution at an intermediate snapshot from one of our simulations. It clearly shows the three peaks corresponding to the three stable gas phases. We also annotate two physically relevant cooling times, namely the local cooling time peak for warm gas phase ($t_{cool,peak}$) and the minimum cooling timescale ($t_{cool,min}$).

The temperature floor is raised to $T_{floor} = 8000$ K for the two-phase gas. The cooling curve is sliced at a temperature lower than the $T_{floor} = 4 \times 10^4$ K in previous works (Das & Gronke (2024); Gronke et al. (2022)) to include the local maxima of the cooling time. We further discuss these multi-phase dynamics more in Section 3.

2.4 Phases of gas

We evaluate the survival of the different phases of gas with different criteria. In the $T_{floor} = 800$ K runs, the mediums are defined as all gas within range:

Cold: $T_{cloud} < T_{cold} < 2 \times T_{cloud}$
Warm: $2 \times T_{cloud} < T_{warm} < T_{mix}$
Hot: $T_{mix} < T_{hot}$

Here, $T_{mix} = \sqrt{T_{cold} \times T_{hot}}$ is the geometric mean of the two gas temperatures initialized in the medium, which has shown to be a good approximation for the mixing physics Kanjilal et al. (2021); Gronke & Oh (2018, 2020); Farber & Gronke (2022). For the the $T_{floor} = 8000$ K runs, the cold gas definition applies for the warm gas instead, since now there are only two phases instead of three.

$$T_{\text{cloud}} = 8 \times 10^2 \text{ K}, \ L_{\text{box}}/R_{\text{cl}} = 50$$
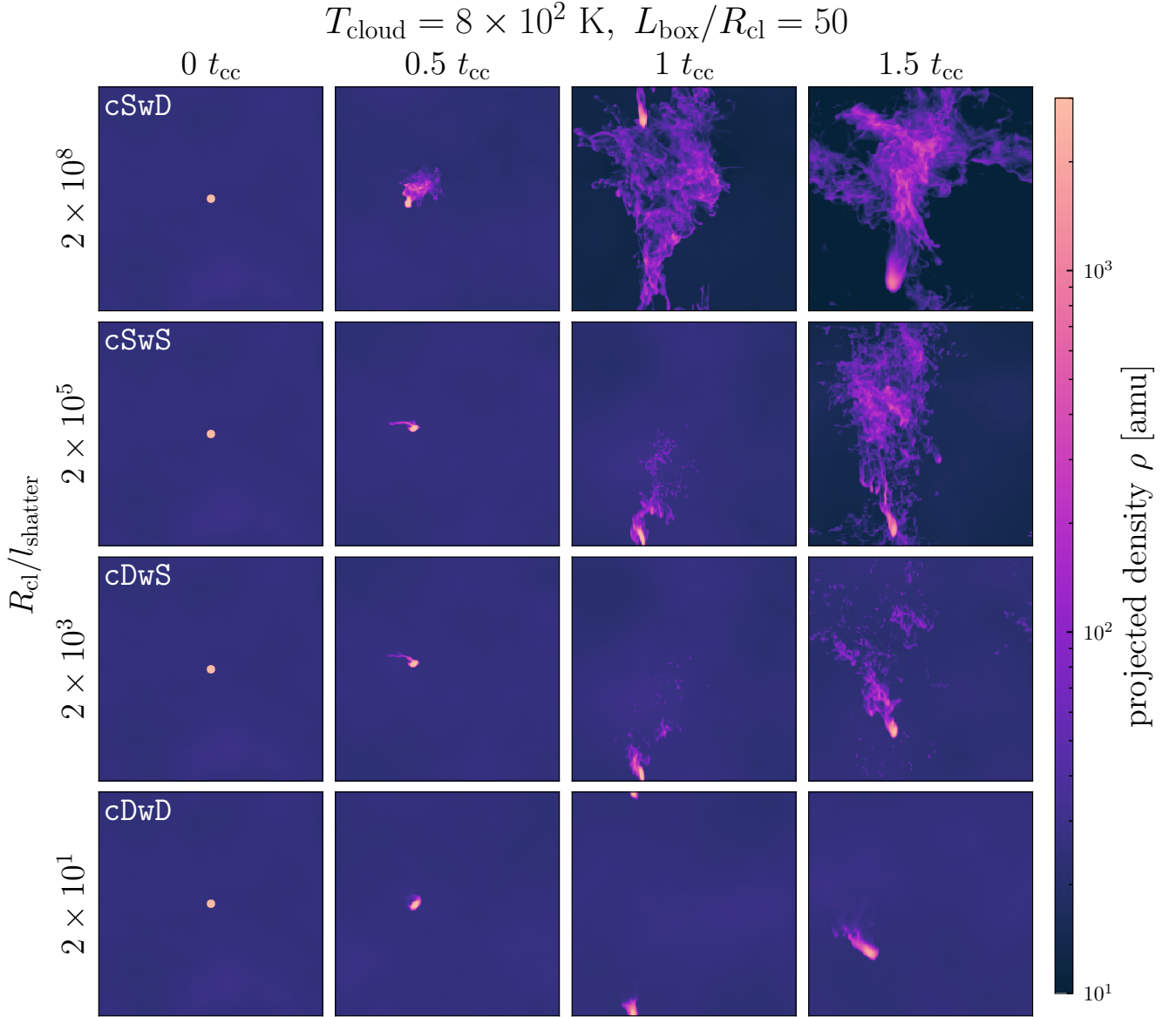
Figure 2. Density projection sums of 800 K clouds, with each row showing boxes of different initial radii (from $R_{\text{cl}} \sim 20 l_{\text{shatter}}$ to $\sim 2 \times 10^8 l_{\text{shatter}}$) and overdensity $\chi \approx 5000$ in the turbulent medium with $\mathcal{M} = 0.4$ and box 50 times the cloud size. Each column shows the cloud growth at different snapshots of the box, corresponding to $t_{\text{cc}} = 0, 0.5, 1$, and 1.5. The colorbar shows the density in amu, where a lighter pink corresponds to denser cold gas regions, purple for mixed warm gas, and blue for the hot gas. Over time, smaller clouds tend to be destroyed and larger clouds survive and grow more cold gas around itself. The plot shows the four regimes of cloud evolution as defined in Section 3.1 and the fragmented morphology of cloud growth.

3 RESULTS: THREE-PHASE GAS

We run turbulent boxes with $\mathcal{M} \approx 0.4, 0.6$, and 0.8 at $T_{\text{floor}} = 800$ K. For each Mach number, we initialize a series of clouds with radii spanning ~ 8 orders of magnitudes, and correspondingly fix the box size to $L_{\text{box}}/R_{\text{cl}} = 20$.

In the following section, we describe the spatial morphology, temperature configurations, and survival-destruction behavior of the cold and warm gas phases in the runs with three phases with $T_{\text{floor}} = 800$ K runs. Most of these results impact the analytical criteria for survival-destruction, which we elaborate on in Section 5.

3.1 Morphology

We begin by examining the spatial morphology of the cold gas. Figure 2 shows the projected density map of four select boxes with the same Mach number, $\mathcal{M} = 0.4,$. Each row contains a cold cloud of different initial size, corresponding to the four survival-destruction regimes. The columns show projections taken at four snapshots corresponding to different multiples of t_{cc}. In each panel for a cloud size at a set time, density of the box is taken at amu and summed along one axis of the box.

In each row of Figure 2, we plot a cloud of size $2 \times 10^1, 2 \times 10^3, 2 \times 10^5$, and $2 \times 10^8 R_{\text{cl}}/l_{\text{shatter}}$. Each choice corresponds to one case characterized by the survival or destruction of either the cold or the warm phase:

$$T_{\text{cloud}} = 8 \times 10^2 \text{ K}, \ L_{\text{box}}/R_{\text{cl}} = 50$$
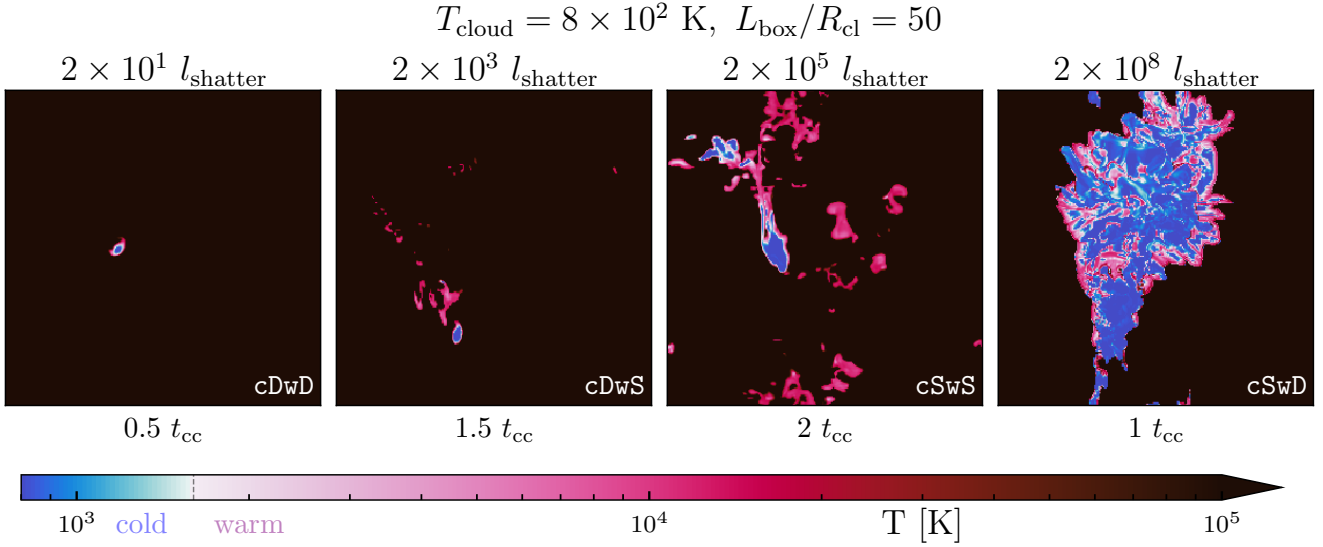
Figure 3. Temperature slices of four 800 K boxes, initialized with clouds of different initial radii (from $R_{\text{cl}} \sim 20 l_{\text{shatter}}$ to $\sim 2 \times 10^8 l_{\text{shatter}}$) and temperature ratio $\chi \approx 5000$ in the turbulent medium with $\mathcal{M} = 0.4$ and box 50 times the cloud size, again representing the four cases of survival-destruction. The slices are taken at snapshots which best demonstrate the evolution of cold gas, with corresponding t_{cc} values shown on the bottom. The diverging colorbar is drawn in a way that shows the different phases of gas as defined in Section 2.4. Going left to right, we see an overall growth of cold medium with the increasing cloud size. Regardless of this, the cold cloud (blue) is always enveloped in layers of warm gas (red), separated from the surrounding hot medium (black).

1. `cDwD`: both cold and warm are destroyed.
2. `cDwS`: cold is destroyed, warm survives.
3. `cSwS`: both cold and warm survive.
4. `cSwD`: cold survives, warm is destroyed.

These four cases correspond to increasing normalized cloud sizes. For the smallest clouds, both the cold and warm gas phases are destroyed by turbulence (`cDwD`). As the cloud size increases, the warm phase begins to survive while the cold phase is destroyed (`cDwS`). With further increases in cloud size, both the cold and warm phases are able to survive (`cSwS`). However, at the largest cloud sizes, warm gas is accreted into the cold gas (`cSwD`).

Additionally, Figure 2 shows that the bigger clouds that survive do not stay compact. Instead, they spatially fragment into small droplets and filaments, which eventually expands to fill the simulated box. Fragmentation of the larger clouds also leads to increased surface area, which accelerates mixing. For a more nuanced discussion of fragmentation, see Gronke et al. (2022); Farber & Gronke (2023); McCourt et al. (2018).

3.2 Temperature distribution

Next, we look at the temperature distributions of different gas phases. We plot the temperature slices of the same four boxes corresponding to the four cases of survival-destruction, to better understand the physical distribution of cold gas. Figure 3 shows the morphology of cold gas and warm gas in the four clouds with different initial radii at different stages of evolution. The temperatures of these two phases correspond to definitions in Section 2.4, with the cold phase being blue, and warm being pink.

As the initial size of the cloud increases from left to right panels, there is more cold gas formation. However, the warm gas is almost always limited to the interface between the cold and hot. For any clump of cold gas, it is always covered by a thin envelope of warm gas. This is consistent with recent conclusions of Blackburn & Farber

(2024)**HD: Cite other earlier papers**, who also saw "intermediate mixing layers" in their simulations. The presence of the intermediate warm gas layer decreases the mixing timescale of cold gas **HD: due to the temperature dependence** $t_{\text{cc}} = \frac{\chi_{\text{cl}}^{1/2} R_{\text{cl}}}{v_{\text{turb}}}$, **where** $\chi_{\text{wc}} = \frac{T_{\text{warm}}}{T_{\text{cold}}}$. **This timescale is mediated by the newly formed warm layer, which is faster than otherwise with direct interaction between hot and cold, due to the decreased** $\chi_{\text{wc}} < \chi_{\text{hw}} < \chi_{\text{hc}}$. We discuss these observations more in depth in the next section.
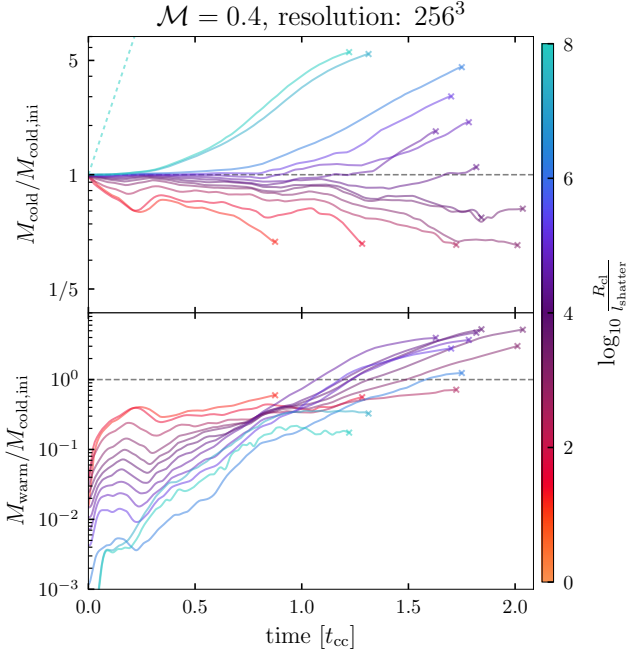
3.3 Survival & destruction

One of the main goals of running small-scale simulations has been to understand how gas of different initial conditions grow and deplete. Here, we define criteria for survival and destruction for both the cold and warm phases, as well as present the corresponding mass evolutions in our simulations.

Since here the gas cloud starts at T_{cloud} with a certain density, we use the ratio of the cold cloud mass from before to after $\sim 5 \, t_{\text{cc}}$. However, since there is initially no warm gas in the box, we instead use the linear slope of its mass evolution to indicate survival / destruction. Note that realistically, the growth of cooler gas phases is seen to be exponential (Gronke et al. 2022).

Figure 4 shows the temporal mass evolution for both cold and warm gases in boxes at $\mathcal{M} = 0.4$. The line colors and colorbar shows the normalized cloud radii of each run. The y-axis shows masses in units of the initial cold gas mass, and the crosses denote where each box achieves stop conditions of $< 20\%$ hot gas mass, $< 5\%$ cold gas mass, or hits pressure floor. Notice also how the stop criteria are reached at different multiples of t_{cc} for boxes with different radii. It is the quickest for the lowest and highest masses, while boxes at intermediate radii tend to survive the longest. This is due to the relative mixing strengths of the different phases.

The cold gas switches from destruction to growth at a critical radius, and its growth increases monotonically with increasing initial
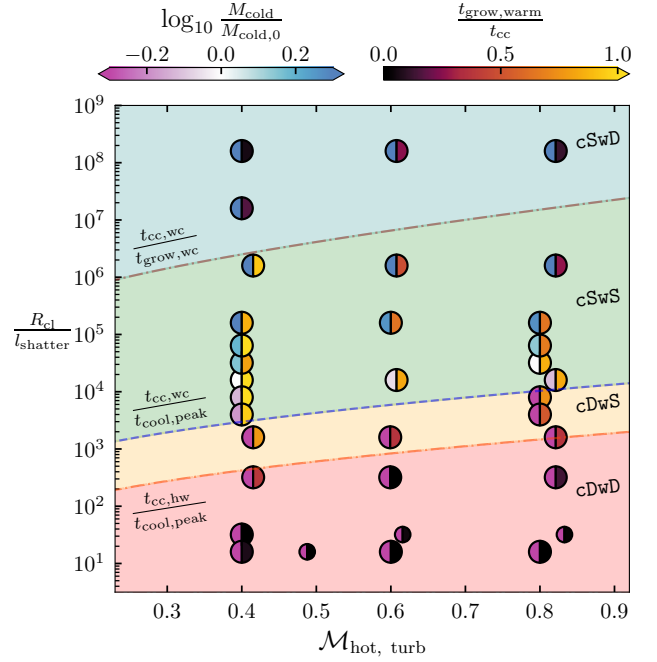
Figure 4. The cold (*top*) and warm (*bottom panel*) gas mass evolution over time in boxes of different initial cloud sizes with $\mathcal{M} = 0.4$, showing destruction and survival relative to the initial cold gas mass on the y-axis. The color of the line indicates normalized cloud size $R_{\rm cl}/l_{\rm shatter}$ of the box, and is also reflected in the diverging colorbar. With increasing box size, cold gas mass tends to turn from destruction to survival. This is however not the case with warm gas, as it dips down again at high cloud radii. Additionally, crosses are plotted at the ends of each box to show the cutoff of mass evolution histories due to stop criteria motivated in Section 2.1. An analytical growth rate is plotted for the largest radii, showing a mismatch with data. Horizontal dashed lines are plotted on both panels at mass = $M_{\rm cold,ini}$.

Figure 5. The parameter distributions of trials with $T_{\rm cloud} = T_{\rm floor} = 800$ K, on Mach number $\mathcal{M}$ and relative cold cloud size $R_{\rm cl}/l_{\rm shatter}$. The filled half-circles show mass evolution of both the cold (*left*) and warm (*right half-circle*) phase for each run, with the corresponding colormap showing mass fractions for cold (*pink / blue*), and the slopes of the mass-time relation for warm gas (*brown / yellow*). This forms four colored regimes: cDwD (pink), cDwS (yellow), cSwS(green), and cSwD (blue). These are separated by three boundary lines, showing the analytical criteria $t_{\rm cc,hw}/t_{\rm cool,peak}$, $t_{\rm cc,wc}/t_{\rm cool,peak}$, and $t_{\rm cc,wc}/t_{\rm grow,wc}$ corresponding to destruction and survival of each gas phase, which is discussed in more detail in Section 5.4. The size of each circle corresponds to its grid resolution.

cloud radius. Unlike the cold gas, the warm gas survival-destruction changes non-monotonically with an increasing cloud radius. At both the lowest and highest cloud radii, the warm gas is unable to grow, represented by a flattened slope. Note that the growth of warm gas is evaluated by the slope of its mass evolution before the cutoff, since its mass almost always increases due to mixing, regardless of $R_{\rm cl}$. For more detailed mass evolution histories of the different cases, see Figure A1.

In Figure 4, we also plot the exponential growth rate based on the expected growth timescale $t_{\rm grow}$ from Gronke et al. (2022) for the run with the largest initial cloud size in dotted line. We find that the cold gas grows much slowly, compared to expected growth rates from two-phase simulations. We present a more nuanced consideration of growth rates in Section 5.1. We also test different criteria for defining the cold gas phase: namely, $T_{\rm cloud} < T < n \times T_{\rm cloud}$, with $n = 2, 3, 5,$ and 10. This results only a marginal change in the quantitative result of the cloud, with conclusions remaining the same.

Given these considerations, we use the definitions of different phases outlined in Section 2.4 to quantify the survival-destruction behaviour for the cold and warm gas in each box. Figure 5 shows the distribution of all $T_{\rm cloud} = 800$ K runs in the parameter space of initial $R_{\rm cl}/l_{\rm shatter}$ and hot gas Mach number $\mathcal{M}$, along with the survival and destruction of the cold and warm phase in left and right halves of the circles, respectively. The survival of cold gas is defined by mass. For the warm gas, we use the mass evolution history in Figure 4 after $1\ t_{\rm cc}$ and before the aforementioned stop conditions. We assume

an exponential growth rate (more details about this assumption in Section 5.1), and fit to the logarithm of warm gas mass over time to get $t_{\rm grow}/t_{\rm cc}$, which we take as the definition for warm gas survival and destruction.

We also plot the analytical lines separating the regimes characterizing the destruction and survival of either gas phases: the analytical criteria $t_{\rm cc,hw}/t_{\rm cool,peak} = 1$, $t_{\rm cc,wc}/t_{\rm cool,peak} = 1$, and $t_{\rm cc,wc}/t_{\rm grow,wc} = 1$. These ratios are formed by cloud crushing times $t_{\rm cc}$ and different cooling $t_{\rm cool}$ and growth $t_{\rm grow}$ timescales of interest. We derive analytical criteria as well as justify the physics for the three boundaries between the regimes in Section 5.2.

Figure 5 shows these lines, which divide the parameter space into the same four distinctive regimes defined in Section 3.1. From the lowest to highest cloud radii, we have cDwD (pink), cDwS (yellow), cSwS(green), and cSwD (blue).

The lines trace the color-code of the points well. The survival-destruction of clouds of the same size also depends weakly on Mach number, which is also reproduced by the analytical lines. Figure 10 discusses this in more detail.

3.4 Tracer scalar evolution

In addition to spatial distributions and growth rate estimates, we use a tracer to track the mass evolution of and exchange between different phases of gas. We implement a scalar quantity, initialized at 1 for all cells containing cold gas, and 0 everywhere else. The scalar shows
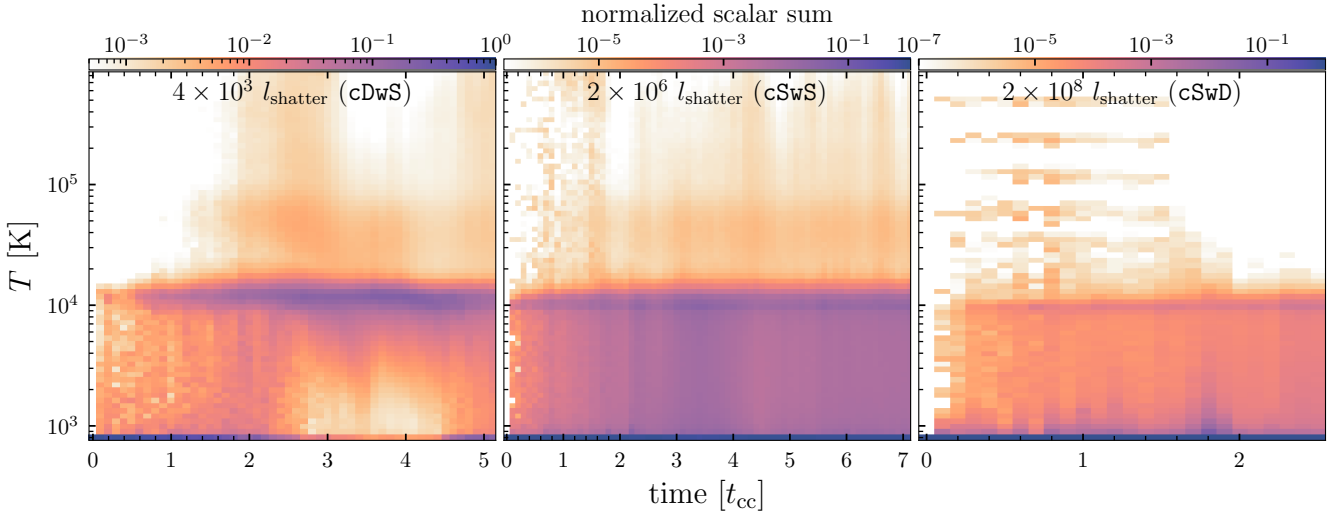
Figure 6. Average density-weighted scalar value of cells in each temperature bin over time, shown in units of t_{cc}. The three panels correspond to cases where either the cold or warm phase survives, as given in Section 3.3. All boxes are $\mathcal{M} = 0.4$. In each box, the scalar value starts as 1 and decays as the cloud mixes with the surrounding medium. The plot shows horizontal bands mapping to the formation of the stable warm phase at $T \sim 1 \times 10^4$ K from the cloud mixing with hot gas. Gas at intermediate temperatures is seen produced from mixing and destroyed by cooling, shown as vertical stretches at different times of the simulation.

the distinct phases of gas, and traces the mixing of the original cloud material into different temperature regimes.

Figure 6 shows the temporal evolution of the density-weighted mean scalar value in all cells within different temperature bins on the y-axis at each snapshot at different times on x-axis. We repeat this for three simulations corresponding to cases cDwS, cSwS and cSwD, i.e. cases where either phases of gas survives. Over time, the scalar values migrate from $T_{cloud} = T_{floor}$ to intermediate temperatures through mixing, forming bands where scalars are spread over a large temperature range.

Case 1 (cDwS): In the leftmost panel, we observe that the scalar values rapidly decay as the cloud begins to mix with the surrounding hot medium. Around $t_{cc} \sim 1$, the scalar values start forming a distinct band near $T \sim 1 \times 10^4$ K. This marks the formation of warm gas from the mixing of cold and hot phases, where the scalar concentration stabilizes as the warm gas survives. The warm gas persists, as cooling is inefficient at this temperature due to the relatively relatively steep t_{cool} cold-ward of the temperature. The large scalar deposit around $T \sim 10^4$ K reflects the significant mass and volume of warm gas that remains after the destruction of the cold phase, which is also evident in Figure 1.

Case 2 (cSwS): In the middle panel, where both warm and cold phases survive, shows the extended stretches of scalar values near $T \sim 800$ K and $\sim 1 \times 10^4$ K. Over time, the scalar mixes into both warm and hot phases, producing vertical bands of color between $\sim 10^3$ K and $\sim 10^6$ K. These vertical stretches are indicative of the mass exchange between the three phases through mixing. However, as cooling dominates, the mixed gas rapidly decays into the stable warm phase, forming the persistent horizontal belt that characterizes the warm phase's survival.

Case 3 (cSwD): In the rightmost panel, the cold phase survives while the warm gas is destroyed. As mixing between cold and hot gas occurs, the mixed gas continues to be driven to lower temperatures via cooling. Most gas eventually cools to T_{floor}, with a minimal warm gas existing as the intermediate mixing layer.

Due to the large presence of warm gas at $T \sim 8000$ K, as well as our observation of hot gas interacting with warm, instead of cold
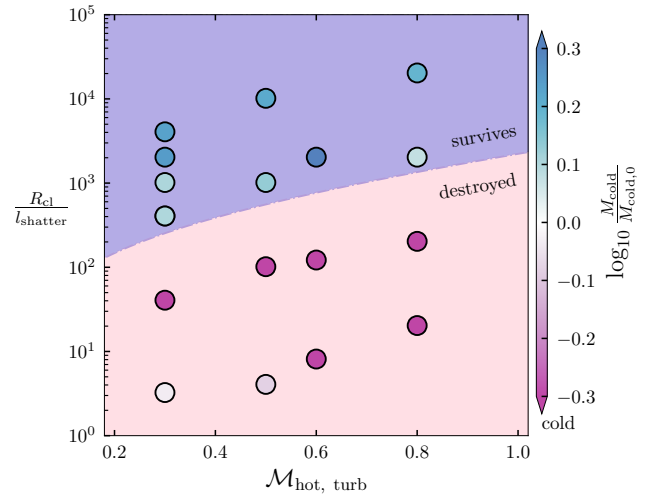
Figure 7. Overview of the two-phase simulations with $T_{cloud} = T_{floor} = 8000$ K, with an analytical expression for the survival/destruction criteria on Mach number $\mathcal{M}$ and normalized cold cloud size $R_{cl}/l_{shatter}$. The boundary maps to the ratio of two timescales $t_{eddy}/t_{cool,mix}$, as noted in Gronke et al. (2022). The colormap shows destruction (*pink*) and survival (*blue*) of the cold gas in the turbulent medium by its final mass. Here the cold gas is defined as $T < 2 \times T_{cloud}$.

gas (Section 3.2), we decided that it would be beneficial to directly investigate the interface of a hot turbulent medium with warm gas at $T = 8000$ K.

Motivated by these results, we run another suite of boxes, raising the temperature floor to $T_{floor} = 8000$ K. We present the results in the section below.

4 RESULTS: TWO-PHASE GAS

We investigate the effect of fixing the temperature floor at $T_{\text{floor}} = 8 \times 10^3$ K. This allows to exclude cold gas and study the interaction between the warm and hot gas. This allows us to test the survival criteria for warm gas, and to corroborate the criterion between two- and three-phase setups.

We sample the parameter space with a range of turbulent hot gas Mach numbers from $\mathcal{M} \in (0, 1)$. Similar to the 3-phase runs, we vary the cloud size, and correspondingly fix the box size to $L_{\text{box}}/R_{\text{cl}} = 20$. Figure 7 gives an overview of this setup represented in the parameter space of $R_{\text{cl}}/l_{\text{shatter}}$ and Mach number $\mathcal{M}$. The color of points represents the final cold gas mass fraction relative to the initial cloud mass, where we define cold gas mass as $T < 2 \times T_{\text{cloud}}$.

In Figure 7, an analytical line separates the runs where the cold gas is destroyed from runs where the cold gas survived. It is given by $t_{\text{cc,hw}}/t_{\text{cool,peak}} = 1$, or $\sim \mathcal{M}_{\text{hot}} \frac{t_{\text{cool,mix}}}{t_{\text{cool,cold}}} 10^{(0.6\mathcal{M})}$. This is generated from the critical $R_{\text{cl}}/l_{\text{shatter}}$ (equivalently $t_{\text{eddy}}/t_{\text{cool,mix}}$) values found in hydrodynamical simulations of Gronke et al. (2022); Das & Gronke (2024) with modifications made for the different temperature floor. We discuss this more in Section 5.3.

5 DISCUSSIONS

5.1 Growth rates

Analytically, the expected growth rate of the cold gas is the mass transfer rate from the warmer phase to the colder phase, which depends on the cold gas surface area and the mixing rate per unit area. This relation is expressed in Equation 1:

$$\dot{m} \sim v_{\text{mix}} A_{\text{cl}} \rho_{\text{hot}} \tag{1}$$

where A_{cl} is the effective cold gas surface area, ρ_{hot} is the surrounding hot gas density, and v_{mix} is the mixing velocity, which has an additional scaling (Gronke & Oh 2020; Fielding et al. 2020; Tan et al. 2021) given by:

$$v_{\text{mix}} \propto (v_{\text{turb,cold}})^{3/4} \left(\frac{L_{\text{cold}}}{t_{\text{cool,cold}}} \right)^{1/4}. \tag{2}$$

Here L_{cold} is the integral scale of turbulence in the cold medium. As seen in Figure 2, the cold gas grows by fragmenting into smaller droplets and filaments. We follow the fractal solution for the limiting case where the cloud continuously fragments down to length scale $\tilde{r}$ (Gronke et al. 2022). This limiting case gives the exponential growth solution:

$$m \sim m_0 \exp(t/t_{\text{grow}}), \tag{3}$$

$$t_{\text{grow}} = \chi \tilde{t}_{\text{cool}} \tag{4}$$

$$= \chi \mathcal{M}^{-1/2} \left(\frac{R_{\text{cl}}}{l_{\text{shatter}}} \right)^{1/2} \left(\frac{R_{\text{cl}}}{L_{\text{box}}} \right)^{-1/6} t_{\text{cool,cold}}. \tag{5}$$

In this parameterization, $\tilde{t}_{\text{cool}}$ is the net cooling time of a turbulent medium, assumed to be the geometric mean of the eddy turnover and cooling time in the cold medium Tan et al. (2021, see their Eq. 25).

With this, we set up exponential fits to the mass evolution histories shown in Figure 4. For each box, we omitted the mass evolution in the first $0.5t_{\text{cc}}$, as the extent of mass growth is similar due to the
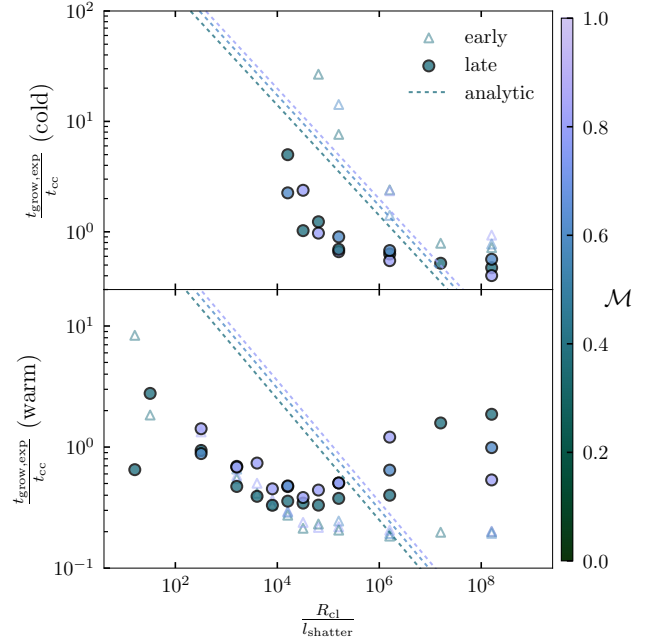

Figure 8. Exponential growth times t_{grow} from the simulation relative to normalized cloud size $R_{\text{cl}}/l_{\text{shatter}}$. Top panel shows cases where cold gas is growing, and bottom panel shows all warm gas runs. For each box, exponential fits were carried out from $0.5t_{\text{cc}}$ until the stop criteria in Section 2.1 is hit. The 'early' (open triangles) and 'late' (colored circles) fits are for first and second half of the valid mass evolution histories. The marker color and the colorbar correspond to the mach number $\mathcal{M}$ of each box, with lighter being higher. The plot also shows three analytic lines corresponding to predicted t_{grow} at each mach number by color.

unavoidable mixing between hot and cold gas. We split $m(t)$ into 'early' and 'late' between $0.5t_{\text{cc}}$ and the stop times described in Section 2.1, and fit an exponential growth time individually. This is done for the warm gas in all boxes, and for the cold gas only when it is growing. Figure 8 presents the fitted growth timescales and their trend with cloud size $R_{\text{cl}}/l_{\text{shatter}}$, with cold and warm presented in two separate panels. Different markers denote the 'early' (open) and 'late' (solid outlined) fits. The plot also shows calculated t_{grow} values from Equation 5 per mach number.

For cold gas in the top panel of Figure 8, t_{grow} shows a clear decreasing trend with increasing radius, which corresponds to faster growth as seen in Figure 4. We note that the early growth rate agrees better with predictions than the late type, which possibly indicates that the cold gas encounters difficulties in mixing due to the depleting hot gas in its later growth stage. This relation also does not seem to have any dependence on mach number.

The bottom panel of Figure 8 shows warm gas t_{grow}. Here it does not evolve linearly with increasing radius, but rather stagnates or decreases for the largest boxes. This is consistent with our previous findings in Section 3.3, where warm gas mixes and cools into cold gas. It is also interesting to compare early and late fits of the warm runs, as the early evolution of warm gas seems to converge after a certain radius. This trend is reflected well in the highest-radii mass evolution histories in Figure 4. Additionally, the calculated t_{grow} relation with cloud radius also breaks down at this point.

We then move on to a more holistic view of growth rate by plotting the fitted t_{grow} values of cold and warm gas against each other. Figure 9 shows the inverse of these values, representing instead the
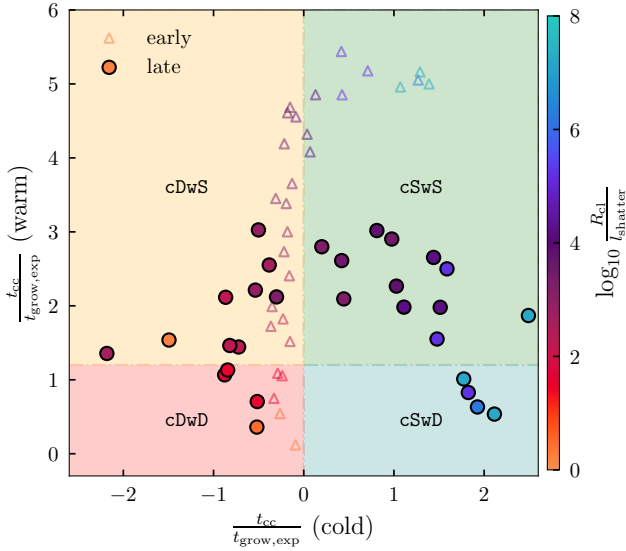
Figure 9. The growth rates of warm and cold gases in each box. Each data point is colored by the normalized cloud size $\log_{10}(R_{\rm cl}/l_{\rm shatter})$. The 'early' (open triangles) and 'late' (colored circles) fits are for first and second half of the valid mass evolution histories described in Figure 8. Similarly, the x-axis represents fitted growth rate $t_{\rm cc}/t_{\rm grow}$ for the cold gas, and the y-axis for warm gas obtained in the same way. Four colored regimes cDwD (pink), cDwS (yellow), cSwS(green), and cSwD (blue) divides the plot, and are discussed in Section 5.4. The boundaries between quadrants are derived from Figure 5. With increasing radius, the points make a U-shape in the plot, corresponding to the growth rate evolutions of either gases.

growth rate, in four quadrants corresponding to the regimes of survival and destruction.

Each point in Figure 9 is positioned based on $t_{\rm grow}$ for cold (x) and warm (y-axis) gases. The colors map to cloud radius, with warmer colors for smaller clouds and cooler colors for larger. The dividing lines between these regimes are based on the analytical criteria further explored in Section 5.4. The distinction between early (open triangles) and late (colored circles) points illustrates how the growth rates evolve over time. Early points tend to be closer to the regime boundaries, indicating the growth for both phases may not yet have stabilized, while the late points cluster within each quadrant. Furthermore, late points show a very clear trend with increasing cloud radii, evolving in a clockwise fashion from lower left (cDwD) to lower right (cSwD). This is because cold gas growth rate starts off low and increases with radius, and the warm gas peaks at medium radii, forming an inverted U-shape in the figure. While the warm gas growth rate tends to flatten for early evolution of high radii boxes, its stagnated growth is a lot more clear in the later stages, as is evident by comparing the right two quadrants.

5.2 Survival-destruction criteria

The goal of our analytical considerations is recovering a criteria on the survival and destruction of each gas phase in the medium. As discussed in Section 3.3, we have limited factors impacting the growth of the cloud to purely the relative timescales for mixing and cooling. Besides this, we also would like to connect these factors1 to quantities pertaining more directly to the simulation setup, such as Mach number $\mathcal{M}$ and cold cloud size $R_{\rm cl}$.

Based on these considerations, we modify the analytical criteria developed in Gronke et al. (2022) and Das & Gronke (2024) to be

more applicable to gas phases at multiple temperatures. We use the following relations to express our parameters in Figure 7 and 5:

$$\mathcal{M} = v_{\rm turb}/c_{\rm s,hot}$$
$$l_{\rm shatter} = t_{\rm cool,min} \cdot c_{\rm s,min}$$
$$t_{\rm eddy} = L_{\rm box}/v_{\rm turb}$$
$$t_{\rm cc} = \frac{\chi_{\rm cl}^{1/2} R_{\rm cl}}{v_{\rm turb}}$$
$$t_{\rm grow} = \chi \mathcal{M}^{-1/2}\left(\frac{R_{\rm cl}}{l_{\rm shatter}}\right)^{1/2}\left(\frac{R_{\rm cl}}{L_{\rm box}}\right)^{-1/6} t_{\rm cool,cold} \quad (6)$$

and therefore, we can express the cold cloud size relative to the shattering length $l_{\rm shatter}$:

$$R_{\rm cl}/l_{\rm shatter} = \frac{R_{\rm cl}}{t_{\rm cool,min} \cdot c_{\rm s,min}}$$
$$= \frac{R_{\rm cl} \cdot \mathcal{M}}{t_{\rm cool,min} \cdot v_{\rm turb}} \frac{c_{\rm s,hot}}{c_{\rm s,min}}$$
$$= \mathcal{M}\frac{t_{\rm cc} \cdot \chi_{\rm cl}^{-1/2}}{t_{\rm cool,min}} \chi_{\rm min}^{1/2}$$
$$= \mathcal{M}\frac{t_{\rm cc}}{t_{\rm cool,min}}\sqrt{\left(\frac{\chi_{\rm min}}{\chi_{\rm cl}}\right)}, \quad (7)$$

where $\chi_{\rm min} = \frac{T_{\rm cloud}}{\chi_{\rm cl}} = \frac{T_{\rm cloud}}{T_{\rm min}} = \omega \approx 1/25$ for $T_{\rm floor} = 800$ K and $\omega \approx 1/1.5$ for the the $T_{\rm floor} = 8000$ K runs. Simplifying and expressing the ratio in terms of $t_{\rm cool}$ and a characteristic timescale:

$$R_{\rm cl}/l_{\rm shatter} = \mathcal{M}_{\rm hot}\frac{t_{\rm char}}{t_{\rm cool,min}}\frac{t_{\rm cc}(\mathcal{M}_{\rm hot})}{t_{\rm char}}\sqrt{\omega}, \quad (8)$$

where $t_{\rm char}$ is the characteristic timescale for the problem. The physical correspondence of this timescale can be split into two cases: The first is $t_{\rm cool,T_0}$ – the cooling time at a temperature of interest. This reflects the characteristic cooling time which competes with $t_{\rm cc}$ – in other words, it is the largest obstacle to cooling to $T_{\rm floor}$, and will be different for each problem. The second case is the growth time $t_{\rm grow}$, of a colder gas in a hotter medium, as calculated using the ratio of the two temperatures. In this case, the mixing process $t_{\rm cc}$ is in competition with the growth, instead of the cooling.

This parameterization clearly shows the physics of the problem, and simplifies it into one with the Mach number $\mathcal{M}$, as expressed below in Equation 10, where $f^1(\mathcal{M})$ is a linear fit:

$$\log_{10}\left(\frac{t_{\rm cc}(\mathcal{M})}{t_{\rm char}}\right) = f^1(\mathcal{M}) \quad (9)$$
$$R_{\rm cl}/l_{\rm shatter} = \mathcal{M}_{\rm hot}\frac{t_{\rm char}}{t_{\rm cool,min}}10^{f^1(\mathcal{M})}\sqrt{\omega} \quad (10)$$

With this parameterization, the survival-destruction criteria of the gas can be expressed in $f^1(\mathcal{M})$, where the cloud survival requires $\frac{t_{\rm cc}(\mathcal{M})}{t_{\rm char}} \gtrsim f^1(\mathcal{M})$, and the opposite for destruction. In other words, $R_{\rm cl}/l_{\rm shatter}$ values larger than the expression given in Equation 10 sees clouds surviving, and smaller values destroyed.

In the coming Sections 5.3 and 5.4, we examine the results of our simulations with the hereby proposed parameterization. Specifically, we will look at how the $t_{\rm cc}$ changes in each case depending on the temperatures of the interacting phases, and identify the characteristic timescales that are in competition. We will identify the linear fit f^1

in each case, and use it to inform the survival-destruction criteria in the Mach number - cloud size parameter space.

5.3 Two-phase Gas

For the two-phase medium, with a cloud initialized at $T_{floor} = 8000\,\mathrm{K}$, we find that the characteristic timescale is a cooling time $t_{char} = t_{cool,T_0}$, which occurs at $T_0 = T_{floor}$. This conclusion is consistent with results of Das & Gronke (2024), which ran the simulations with a higher temperature floor at $4 \times 10^4\,\mathrm{K}$ to imitate the high cooling time (t_{cool}) at these temperatures. Figure 7 shows the resulting analytical destruction-survival criteria.

The choice of this timescale is physically motivated, as the corresponding temperature reflects the maximum cooling time in the temperature range between T_{warm} and T_{floor}. As such, the temperature also reflects the largest limiting timescale in the cooling process.

One more observation we made is that the correct analytical relation is only produced when the mixed gas temperature is calculated using the temperature of the lowest t_{cool}, as opposed to the temperature of the cloud. Physically, this means that the bulk of the cold gas phase that mixes with the hot gas sits at $T(t_{cool,min}) \sim 1 \times 10^4\,\mathrm{K}$ – not at the floor temperature. Figure 1 also supports this conclusion as the number of cells peak at the trough of the cooling time curve. The same applies to Section 3.4 and Figure 6, which shows the warm gas at $t_{cool,min}$ mixing with the hot gas, producing spikes of scalar values at the new $T_{mix} \approx$. Though both analyses are for the 800 K runs, the same conclusions apply here.

The above observation is consistent with results of Farber & Gronke (2022), which noticed that gas of slightly higher temperature than the cloud tends to survive longer, due to interaction of t_{cool} and t_{cc} values. This observation is unique to the $8 \times 10^3\,\mathrm{K}$ runs, due to the lower temperature floor allowing for the cold gas to cool to a regime with higher t_{cool}.

To summarize, our conclusions for the $T_{floor} = 8000\,\mathrm{K}$ runs are as follows:

1. We are able to replicate the analytical conclusions of Das & Gronke (2024). We test that the analytical boundaries for survival-destruction using timescales also work for simulations with different physical parameters.

2. We show that exerting a temperature floor is a good way to simplify the system, while representing the high cooling time at low temperatures. This is significant as the lower $T_{floor} = 8000\,\mathrm{K}$ in our setup will allow the gas to cool to a more naturally stable phase. As the results of Das & Gronke (2024) are replicated, we then postulate that the $T_{floor} = 800\,\mathrm{K}$ floor will also be a good approximation of the physics mentioned in Section 2.3.

3. We investigate the interaction between warm and hot gases in our $T_{floor} = 800\,\mathrm{K}$ simulations. This is motivated by the large volume-fraction of warm gas, concentrated at $T \sim 1 \times 10^4\,\mathrm{K}$. The results are identical between the two temperature floors, which informs our discussions in Section 5.4.

5.4 Three-phase Gas

JW: Phase structures; Interface; Use those timescales; Go line by line; Refer to scalar

Comparatively, the three-phase medium with $T_{floor} = 800\,\mathrm{K}$ is a lot more difficult to analyze. Due to the interface of three gases, the timescales become more complex to model.

With this in mind, we fit lines f^1 that corresponds to the survival-destruction criteria of the cold gas, as well as two others that maps to
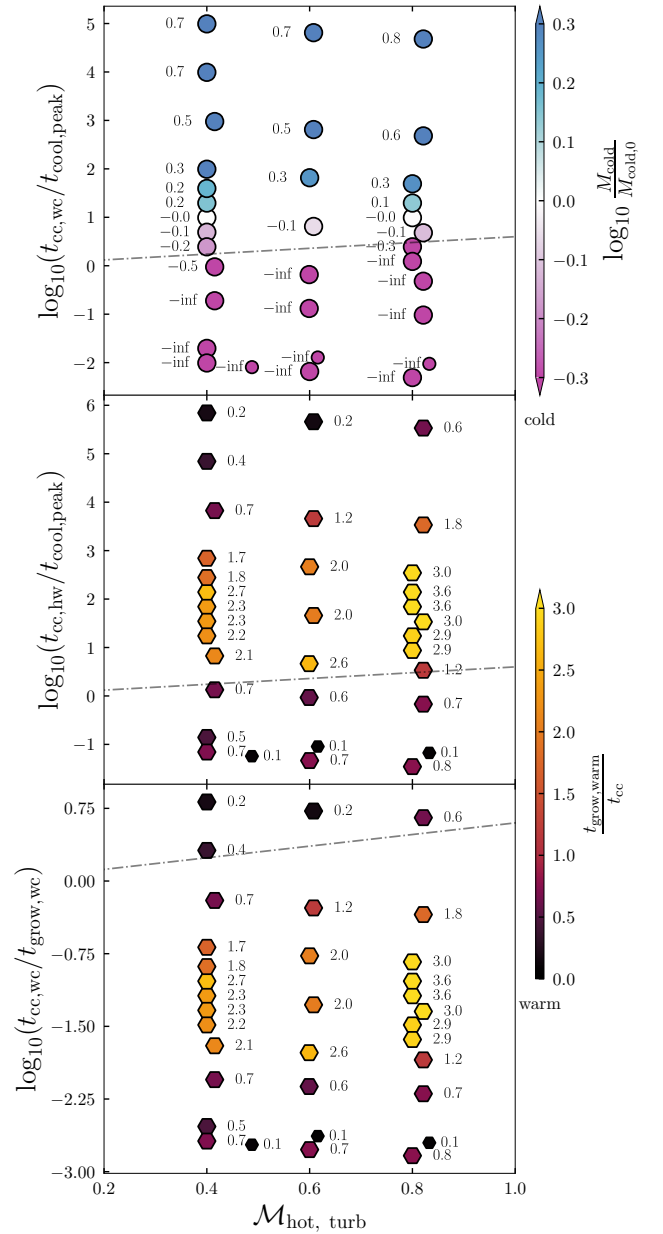
Figure 10. An overview of the $T_{cloud} = 800\,\mathrm{K}$ runs in the parameter space of Mach numbers $\mathcal{M}$ and timescale ratios. *Left panel*: $t_{cc,wc}/t_{cool,peak}$ for cold; *Middle panel*: $t_{cc,hw}/t_{cool,peak}$ for warm-hot interaction; and *right panel*: $t_{cc,wc}/t_{grow,wc}$ for warm-cold interaction. Each point is color-coded to represent survival-destruction behaviors of the cold gas by final/initial mass fraction, or the warm gas by the slope of mass evolution over time. Each panel also shows a linear analytical line $f^1 = 0.6 \times \mathcal{M}$ of survival and destruction criteria.

the appearance and re-disappearance of the warm medium. The result of these fits can be seen in Figure 5 and 10, along with points representing runs in the Mach number – timescales parameter space. In the following subsections, we make an effort to explain the timescales we had used for each case, as well as motivate each of the choices, and explore the physical significance.

5.4.1 Warm-hot interaction

The behavior of the warm medium ($T \sim 8000$ K) in a hot, turbulent environment is similar to that of the two-phase cold gas with $T_{\mathrm{cloud}} = 8000$ K. As noted in Section 3, the growth of cold gas always comes after the warm gas has filled the box. Therefore, our observations here are to be expected, as the interaction between the warm and cold phases would not come into play until the warm gas has grown sufficiently. One can effectively ignore the cold gas in this regime, and use the same timescales in Section 5.3.

As a result, we use the cloud crushing time between hot and warm phase $t_{\mathrm{cc,hw}}$, as well as $t_{\mathrm{cool},T_0} = t_{\mathrm{cool},8000\,\mathrm{K}}$, which is the same timescale used in Section 3. In reference to Equation 10, we plot the analytical line in the middle panel of Figure 10. We discover that the linear fit of $f^1 \approx 0.6 \times \mathcal{M}$ in Gronke et al. (2022) still holds. For consistency, this line is also used for the two other cases.

Figure 10 as well as f^1 parameterization seem to indicate a weak exponential Mach number dependence of the analytical criteria, in additional to the linear dependence already in Equation 10. Gronke et al. (2022) attributed this to a more violent fragmentation and subsequent dispersion of the cold gas in boxes with stronger Mach numbers, and justified this with timescale ratios such as $t_{\mathrm{grow}}/t_{\mathrm{eddy}} \propto \mathcal{M}^{1/2}$, which reflects the recovery of the cloud between being hit by subsequent shocks. This dependence is also replicated in the analytical lines of the other two boundaries.

5.4.2 Cold gas survival/destruction

As discussed in Section 3.2, the growth of the cold cloud (which, as a reminder, develops after the growth of warm gas) is always enveloped in a layer of warm gas. This physical configuration is also found in the recent work by Blackburn & Farber (2024), where the cold gas grows from the intermediate warm phase, instead of interfacing with the hot phase directly. This results in a faster mixing rate due to the lower temperature ratio between the two interacting gas phases.

Due to this phenomenon, we use instead the cloud crushing time between warm and cold $t_{\mathrm{cc,hw}}$, and keeping $t_{\mathrm{cool},T_0} = t_{\mathrm{cool},8000\,\mathrm{K}}$ the same. This results in the points being shifted downward in the parameter space, where the f^1 approximation also works for this case.

5.4.3 Warm-cold interaction

As discussed previously in Section 5.4.2, warm gas forms first in our simulations, from which the cold gas can grow. This is still the case for runs with the largest cloud radii, where cooling is much more efficient than the turbulent mixing. Here, any warm gas would be converted into cold gas almost immediately. As such, we see a thin, growing layer of warm gas surrounding the newly-formed cold gas, not dissimilar to the intermediate mixing layers found in Blackburn & Farber (2024).

Modeling the physics in these cases was most difficult, as many more timescales have to be taken into account compared to the previous case. We eventually find the ratio of mixing $t_{\mathrm{cc,wc}}$ and growth timescale $t_{\mathrm{grow,wc}}$ between the warm and cold gas to be a good criteria for the cooling of warm gas into the cold clouds.

This is an interesting conclusion, as the t_{grow} defined in Section 5.1 already accounts for the mixing timescale. Thus, one can argue that this comparison is unphysical. We do think there are timescales that better reflect the physics of the cold-warm interactions, as well as other ways to express the survival-destruction criteria. We consider these points to expand on in future works.

JW: Expand on this part

One more caveat of this configuration is that there will always be some warm gas at most points in the simulation. However, as soon as the hot gas in the box inevitably runs out, the warm gas disappears as there is no further channel of mixing, and the entire box mixes into the cold phase.

5.5 Connections to previous studies

Connections to previous studies

5.6 Limitations and future work

Future work

6 CONCLUSIONS

In this paper, we use small-scale hydrodynamical simulations to explore the behavior of multiphase gas in a turbulent box. We tested clouds at two temperatures: $T_{\mathrm{cloud}} = 8000$ K and 800 K – corresponding to two stable gas phases in the CGM – and explored respective survival and destruction criteria for each.

We hypothesize that the interface between the physical processes in the multiphase CGM can be mapped to the interaction of different timescales, such as cooling for t_{cool}, mixing for t_{cc}, and the growth of gas for t_{grow}. From this, we developed analytical predictions on the survival-destruction behaviors of the cold gas in the turbulent, hot medium based on timescale ratios. We also found a Mach number $\mathcal{M}$ dependence in the survival and destruction of the different gas phases, which could be attributed to the fragmentation and dispersion of cold gas, and is consistent with conclusions of previous simulations (Gronke et al. 2022).

Our main conclusions are:

1. The survival and destruction of the 800 K cold cloud in a hot, turbulent medium depends on its size relative to the shattering length l_{shatter}. Smaller clouds tends to be destroyed, while larger clouds grow in fragmented droplets, as consistent with observations of Gronke et al. (2022); Farber & Gronke (2023); McCourt et al. (2018).

2. The cold cloud grows by mixing with the surrounding hot medium, as is evident from the tracer scalar distributions. This mixing creates an intermediate warm layer at ~ 8000 K, which has a lower temperature contrast. As such, the warm phase interacts with both the cold and the hot, and reduces the mixing timescale. This is supported by conclusions of Blackburn & Farber (2024).

3. The survival and destruction of the warm phase in the hot medium can be recreated by simulations with a $T_{\mathrm{floor}} = T_{\mathrm{cloud}} = 8000$ K setup. While the growth of cold phase depends on its interaction with the warm phase, not the hot medium.

and the University of Chicago CCRF's Metcalf Research Fellowship Grant program.

This project makes use of the `Athena`++ (Stone et al. 2020). Computations were performed on the Freya HPC system at the Max Planck Computing and Data Facility. Analyses presented in this paper were additionally aided by the following free software packages: `NumPy` (Harris et al. 2020), `SciPy` (Jones et al. 01), `Matplotlib` (Hunter 2007), `yt` (Turk et al. 2011), and `GitHub`. We have also used the Astrophysics Data Service (`ADS`) and `arXiv` preprint repository extensively during this project and the writing of the paper.

DATA AVAILABILITY

Data related to this work will be shared on reasonable request to the corresponding author.

REFERENCES

Bennett J. S., Sijacki D., 2020, MNRAS, 499, 597
Blackburn M. G., Farber R. J., 2024, Research Notes of the American Astronomical Society, 8, 94
Das H. K., Gronke M., 2024, MNRAS, 527, 991
Eswaran V., Pope S. B., 1988, Computers and Fluids, 16, 257
Farber R. J., Gronke M., 2022, MNRAS, 510, 551
Farber R. J., Gronke M., 2023, MNRAS, 525, 1839
Faucher-Giguère C.-A., Kereš D., Dijkstra M., Hernquist L., Zaldarriaga M., 2010, ApJ, 725, 633
Fielding D. B., Ostriker E. C., Bryan G. L., Jermyn A. S., 2020, ApJ, 894, L24
Gronke M., Oh S. P., 2018, MNRAS, 480, L111
Gronke M., Oh S. P., 2020, MNRAS, 492, 1970
Gronke M., Oh S. P., Ji S., Norman C., 2022, MNRAS, 511, 859
Harris C. R., et al., 2020, Nature, 585, 357
Hummels C. B., et al., 2019, ApJ, 882, 156
Hunter J. D., 2007, Computing In Science & Engineering, 9, 90
Jones E., Oliphant T., Peterson P., et al., 2001–, SciPy: Open source scientific tools for Python, http://www.scipy.org/
Kanjilal V., Dutta A., Sharma P., 2021, MNRAS, 501, 1143
McCourt M., Oh S. P., O'Leary R., Madigan A.-M., 2018, MNRAS, 473, 5407
Nelson D., et al., 2020, MNRAS, 498, 2391
Schmidt W., Hillebrandt W., Niemeyer J. C., 2004, arXiv e-prints, pp astro–ph/0407616
Stone J. M., Tomida K., White C. J., Felker K. G., 2020, ApJS, 249, 4
Tan B., Oh S. P., Gronke M., 2021, MNRAS, 502, 3179
Townsend R. H. D., 2009, ApJS, 181, 391
Tumlinson J., Peeples M. S., Werk J. K., 2017, ARA&A, 55, 389
Turk M. J., Smith B. D., Oishi J. S., Skory S., Skillman S. W., Abel T., Norman M. L., 2011, ApJS, 192, 9
van de Voort F., Springel V., Mandelker N., van den Bosch F. C., Pakmor R., 2019, MNRAS, 482, L85

APPENDIX A: DETAILED MASS EVOLUTION

We show the fractional mass evolution of different phases of four runs in Figure A1, corresponding to four different regimes of gas phase survival-destruction. All runs are taken at $\mathcal{M} = 0.8$ for different normalized initial cloud sizes.
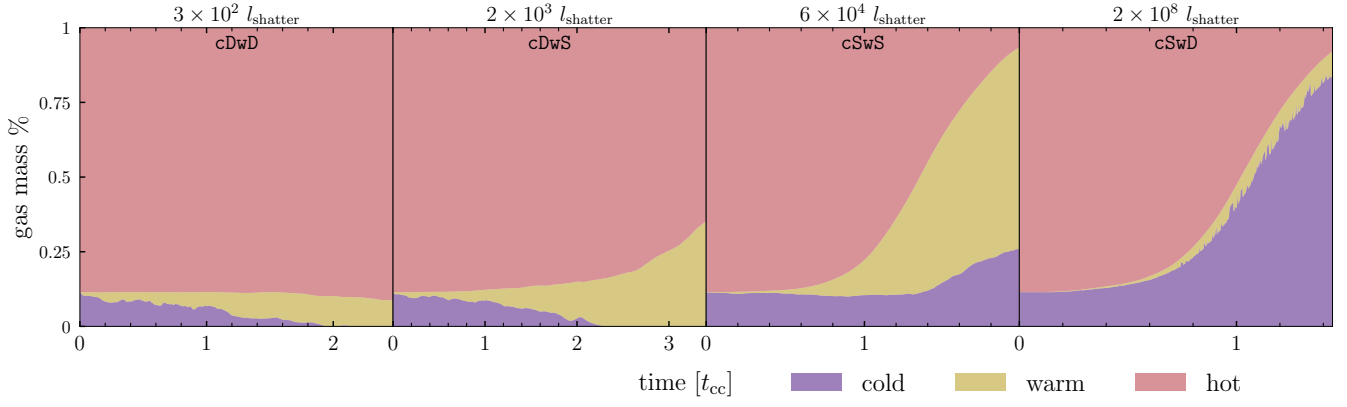
Figure A1. Each panel shows the percentage of mass in the cold, warm, and hot gas phases of the box over time for a single run. Each run is chosen to fall in a different regime of the parameter space as given in Section 3.3, showing destruction and survival of warm, cold, and hot gases, respectively.